Inorganic Chemistry

Article

pubs.acs.org/IC

Thermal Spin Crossover and LIESST Effect Observed in Complexes $[Fe(L^{Ch})_2(NCX)_2]$ [L^{Ch} = 2,5-Di(2-Pyridyl)-1,3,4-Chalcadiazole; Ch = O, S, Se; X = S, Se, BH_3]

Julia Klingele,*[,†] Dominic Kaase,[†] Maximilian Schmucker,[†] Yanhua Lan,[‡] Guillaume Chastanet,[§] and Jean-François Létard[§]

[†]Institut für Anorganische und Analytische Chemie, Albert-Ludwigs-Universität Freiburg, Albertstrasse 21, D-79104 Freiburg, Germany

[‡]Institut für Anorganische Chemie, Karlsruher Institut für Technologie (KIT), Engesserstrasse 15, Geb. 30.45, D-76131 Karlsruhe, Germany

[§]CNRS, Univ. Bordeaux, Institut de Chimie de la Matière Condensée de Bordeaux (ICMCB), UPR 9048, Groupe des Sciences Moléculaires, 87, Av. Doc. A. Schweitzer, F-33608, Pessac, Francee

Supporting Information

ABSTRACT: Two new complexes belonging to the family $[Fe^{II}(\mathbf{L})_2(NCX)_2]$ have been synthesized and structurally characterized. Complexation of the ligand $\mathbf{L^O}$ = 2,5-di(2-pyridyl)-1,3,4-oxadiazole results in the formation of two derivatives of $[Fe^{II}(\mathbf{L^O})_2(NCS)_2]$ (**1**) with the common s-trans and the rarely observed s-cis conformation. No thermal spin crossover (SCO) was observed for the amorphous bulk material of the mixture. Using the new ligand $\mathbf{L^{Se}}$ = 2,5-di(2-pyridyl)-1,3,4-selenadiazole, compound $[Fe^{II}(\mathbf{L^{Se}})_2(NCS)_2]$·1.4DCM·0.6MeOH (**2**·1.4DCM·0.6MeOH) was structurally characterized by single crystal X-ray diffraction. Bulk material of $[Fe^{II}(\mathbf{L^{Se}})_2(NCS)_2]$·MeOH (**2**·MeOH) exhibits a thermally induced SCO with small hysteresis [$T_{1/2}(\downarrow)$ = 91 K, $T_{1/2}(\uparrow)$ = 96 K]. LIESST and reflectivity studies have been performed on the SCO complexes $[Fe^{II}(\mathbf{L^S})_2(NCS)_2]$, $[Fe^{II}(\mathbf{L^S})_2(NCSe)_2]$, $[Fe^{II}(\mathbf{L^S})_2(NCBH_3)_2]$·$H_2O$ [$\mathbf{L^S}$ = 2,5-di(2-pyridyl)-1,3,4-thiadiazole], and **2**·MeOH. All complexes belong to the T_0 = 90 K line [T(LIESST) = $T_0 - 0.3T_{1/2}$]. $[Fe^{II}(\mathbf{L^S})_2(NCS)_2]$, that exhibits a two-stepped thermal SCO process, has been found to also exhibit two well-separated T(LIESST) temperatures [T(LIESST, 1) = 44 K; T(LIESST, 2) = 53 K].

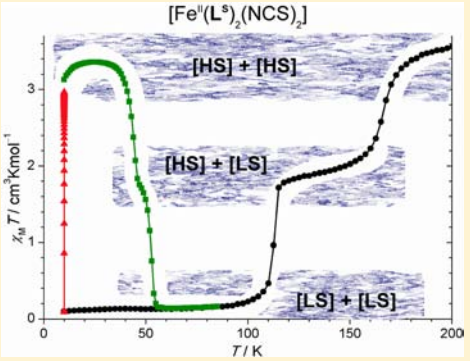

INTRODUCTION

The spin-crossover (SCO) phenomenon is a very intensively studied switching process found in coordination compounds. In thermally induced SCO processes, complexes switch their spin state from high-spin (HS) to low-spin (LS) on cooling the sample. On a first approach, the SCO properties of a compound depend on the ligand field (LF), imposed to the metal ion by the surrounding donor atoms. Simplifying, one can state that the stronger the ligand, the higher the ligand field, and the higher the SCO temperature $T_{1/2}$.[1] Recently we have illustrated this effect on iron(II) complexes of ligand 2,5-di(2-pyridyl)-1,3,4-thiadiazole ($\mathbf{L^S}$).[2] In the $[Fe^{II}(\mathbf{L^S})_2(NCX)_2]$ family (X = S, Se, BH_3), a shift of $T_{1/2}$ toward high temperature was observed on going from NCS^- to $NCSe^-$ and $NCBH_3^-$, in agreement with the increase of the ligand field strength along the NCS^- < $NCSe^-$ < $NCBH_3^-$ spectrochemical series. But obviously, not only LF governs the SCO properties—packing effects also play a significant role in solid SCO compounds.[3−5] Subtle packing effects, like H-bonds,[6] $\pi-\pi$-stacking, or other short contacts between neighboring units[7] may also influence $T_{1/2}$, but mainly they model the type of SCO through cooperative interactions and may give rise to abrupt SCO curves or cause hysteresis. In that sense, complex $[Fe^{II}(\mathbf{L^S})_2(NCS)_2]$ (**A**) for example has been found to undergo a thermally induced abrupt two-step SCO curve;[8] whereas in $[Fe^{II}(\mathbf{L^S})_2(NCSe)_2]$ (**B**) and $[Fe^{II}(\mathbf{L^S})_2(NCBH_3)_2]$·$H_2O$ (**C**·H_2O), only one SCO step is observed with more gradual character.[2]

Apart from using temperature changes, the SCO process may also be triggered by light irradiation, this process being called the LIESST effect (light-induced excited spin-state trapping).[9,10] The lifetime of the thereby produced metastable photoinduced HS state may be very long at low temperature but becomes very short for temperatures above the limiting temperature T(LIESST).[11] It has been found, that the temperature T(LIESST) strongly depends on $T_{1/2}$ of the thermally induced SCO process of the same compound, following the linear equation: T(LIESST) = $T_0 - 0.3T_{1/2}$ (Figure 1).[12,13] Also it has been found that T(LIESST) is not

Received: February 9, 2013
Published: April 26, 2013

   dx.doi.org/10.1021/ic400342m | *Inorg. Chem.* 2013, 52, 6000−6010

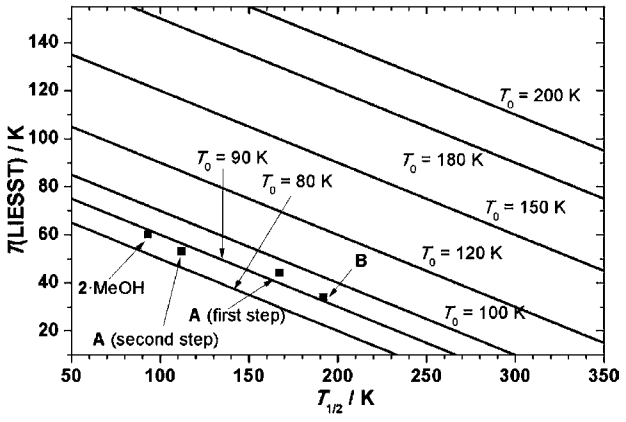

Figure 1. T(LIESST) vs $T_{1/2}$ plots of selected T(LIESST) = $T_0 - 0.3T_{1/2}$ lines. The full squares symbolize the data of the complexes **2**·MeOH, **A** (first and second step), and **B**, considered in this paper.

as dependent on intermolecular cooperativity as $T_{1/2}$ and that it mainly depends on the coordination environment of the metal ion.[14−16] Therefore in the linear equation for T(LIESST), T_0 is usually characteristic for the type of complex studied. Co−Fe Prussian Blue analogues,[17] for example, will follow the line of another T_0 than complexes belonging to the family $[Fe^{II}(bpp)_2](X)_2{\cdot}nH_2O$ [bpp = 2,6-bis(pyrazol-3-yl)-pyridine].[13] However, this is not always the case as recently reported on mononuclear compounds[18] for reasons that are still to be understood. Regarding multistep spin-crossover behavior in mononuclear,[8,19−25] polynuclear,[26,27] or polymeric[28−35] compounds, the main observation regarding the LIESST effect is that the presence of steps in the thermal spin-crossover curve does not systematically induce stepped T(LIESST) curves. This could mainly be followed from the fact that because of the T(LIESST) = $T_0 - 0.3T_{1/2}$ relationship the difference between the various $T_{1/2}$ has to be very large to observe steps in the T(LIESST) curve. A gap of 20 K between two temperatures $T_{1/2}$ corresponds to only 6 K of difference between the two corresponding T(LIESST) values, which is hardly observed. On the other hand the absence of steps in the T(LIESST) curve does not preclude the observation of stepped isothermal relaxation kinetics, as it has been shown on dinuclear 2,2′-bipyridine-bridged complexes.[27] But, when both T(LIESST) and thermal spin-crossover curves are stepped, the [T(LIESST), $T_{1/2}$] couples are placed on the T(LIESST) vs $T_{1/2}$ database in agreement with the T(LIESST) = $T_0 - 0.3T_{1/2}$ relationship: the higher $T_{1/2}$, the lower T(LIESST).

Summarizing, prediction of LIESST behavior on thermal multistep spin-crossover compounds is not an easy task. In that sense, the present article aims at investigating the photomagnetic properties of the recently reported SCO family of the type $[Fe^{II}(L^S)_2(NCX)_2]$ (X = S, Se, $NCBH_3$).[2,8] Two new complexes were added to this family, featuring 2,5-di(2-pyridyl)-1,3,4-oxadiazole (L^O) or 2,5-di(2-pyridyl)-1,3,4-selenadiazole (L^{Se}) instead of L^S and NCS^- as the coligand.

RESULTS AND DISCUSSION

Synthesis of the New Complexes $[Fe^{II}(L^O)_2(NCS)_2]$ (1) and $[Fe^{II}(L^{Se})_2(NCS)_2]$ (2). For the synthesis of 2,5-di(2-pyridyl)-1,3,4-oxadiazole (L^O) in multigram quantity, the indirect synthesis via 3,6-bis-(2-pyridyl)-dihydrotetrazine (**III**), following a literature procedure of Geldard and Lions,[36] turned out to be the most efficient of all tested synthetic routes (Scheme 1).

The new ligand 2,5-di(2-pyridyl)-1,3,4-selenadiazole (L^{Se}) was synthesized from pyridine-2-carboxylic acid *N*′-(pyridine-2-carbonyl)-hydrazide (**II**) with woollins' reagent, modifying a literature procedure for the synthesis of 2,5-disubstituted 1,3,4-selenadiazoles.[37] Contrary to the described procedure by Hua and Woollins for benzyl-substituted derivatives of L^{Se}, it was found that a reaction time of 7 h did not suffice to carry out the reaction successfully. Instead the reaction mixture was refluxed for 24 h and the resulting orange suspension was purified with column chromatography under argon atmosphere giving the ligand as a slightly purple solid in moderate yield (Scheme 1). Choosing noninert conditions and nonabsolute solvents resulted in its decomposition. Purified L^{Se} is stored and handled under an inert atmosphere and absence of light. A single crystal of L^{Se} suitable for X-ray analysis was obtained by recrystallization from ethyl acetate (Figure S1, Supporting Information). Hydrazide **II** was synthesized by reacting 2-picolinoylchloride hydrochloride with pyridine-2-carboxylic acid hydrazide (**I**),[38] synthesized from methyl pyridinecarboxylate[39] and hydrazine monohydrate (Scheme 1).

Reactions of L^O and L^{Se} with "$Fe(NCS)_2$" using a 2:1 molar ratio in MeOH solution and slow diffusion techniques, resulted

Scheme 1. Synthesis of 2,5-Di(2-pyridyl)-1,3,4-selenadiazole (L^{Se}), 2,5-Di(2-pyridyl)-1,3,4-oxadiazole (L^O), and Their Iron(II) Complexes $[Fe^{II}(L^{Ch})_2(NCS)_2]$ (1) Ch = O; (2) Ch = Se[a]

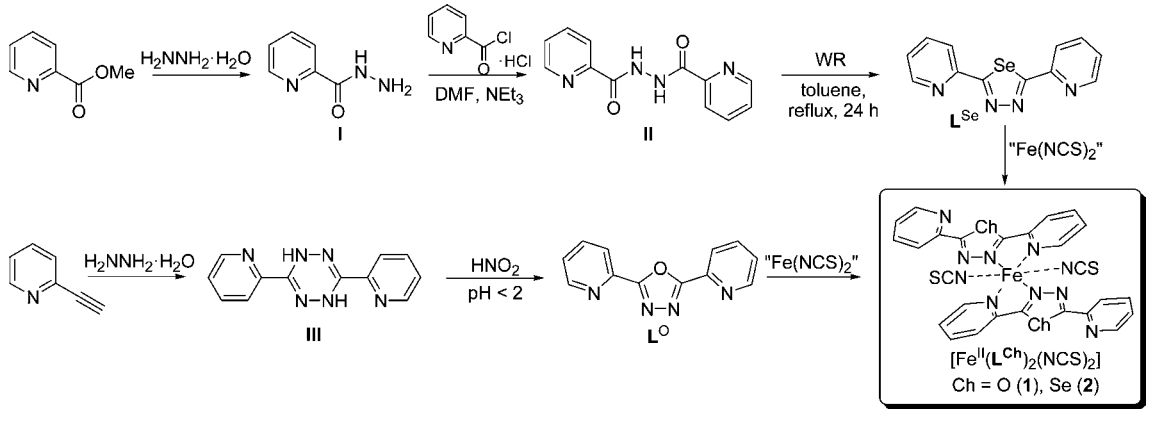

[a]WR = Woollins' reagent.

dx.doi.org/10.1021/ic400342m | *Inorg. Chem.* 2013, 52, 6000−6010

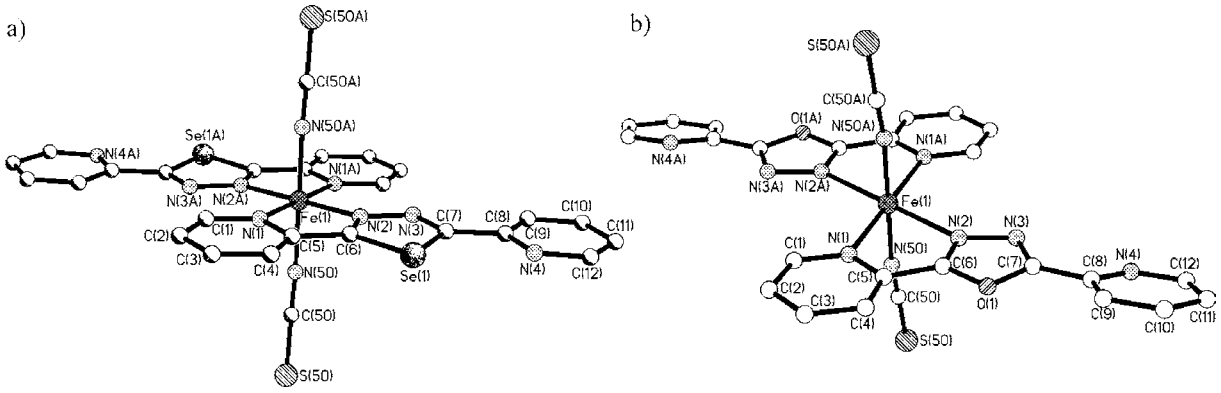

Figure 2. (a) View of the molecular structure of $[Fe^{II}(L^{Se})_2(NCS)_2 \cdot 1.4DCM \cdot 0.6MeOH$ (**2**·1.4DCM·0.6MeOH). Hydrogen atoms and solvent molecules have been omitted for clarity. Symmetry operation used to generate equivalent atoms: (A) $-x, -y, -z + 2$; (b) view of the molecular structure of $[Fe^{II}(L^{O})_2(NCS)_2]$ (**1b**) with emphasis on the ligands in the s-cis configuration.

Scheme 2. Series of Five Related Complexes $[Fe^{II}(L^{Ch})_2(NCX)_2]$ (Ch = O, S, Se; X = S, Se, BH_3)

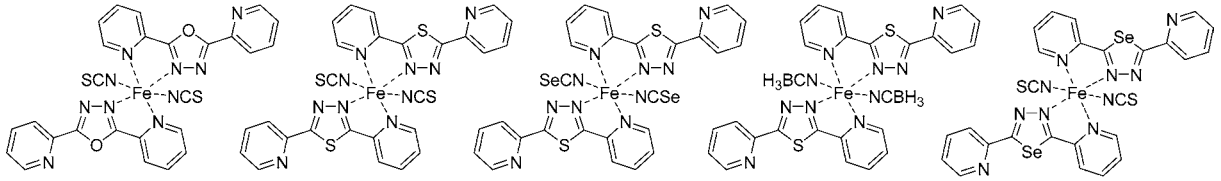

$[Fe^{II}(L^{O})_2(NCS)_2]$ (**1**) $[Fe^{II}(L^{S})_2(NCS)_2]$ (**A**) $[Fe^{II}(L^{S})_2(NCSe)_2]$ (**B**) $[Fe^{II}(L^{S})_2(NCBH_3)_2]$ (**C**) $[Fe^{II}(L^{Se})_2(NCS)_2]$ (**2**)

in the formation of dark red and green crystalline compounds, identified as $[Fe^{II}(L^{O})_2(NCS)_2]$ (**1**) and $[Fe^{II}(L^{Se})_2(NCS)_2] \cdot 1.4DCM \cdot 0.6MeOH$ (**2**·1.4DCM·0.6MeOH) (Figure 2a) by single crystal X-ray diffraction, respectively (Scheme 1). Compound $[Fe^{II}(L^{O})_2(NCS)_2]$ (**1**) was identified to exist in two isomeric configurations, where the pyridyl nitrogen atoms either point in opposite directions (**1a**) as in **2**·1.4DCM·0.6MeOH (Figure S2, Supporting Information) or in the same direction (**1b**, Figure 2b). Amorphous bulk material of $[Fe^{II}(L^{O})_2(NCS)_2]$ (**1**) was obtained under identical reaction conditions but stirring the reaction mixture until precipitation was complete. After drying the crystalline material **2**·1.4DCM·0.6MeOH in vacuo bulk material was obtained, which is best formulated as **2**·MeOH, according to elemental analysis.

The series $[Fe^{II}(L^{Ch})_2(NCX)_2]$ (Ch = O, S, Se; X = S, Se, BH_3) comprising of five related iron(II) complexes, namely $[Fe^{II}(L^{O})_2(NCS)_2]$ (**1**), $[Fe^{II}(L^{S})_2(NCS)_2]$ (**A**), $[Fe^{II}(L^{S})_2(NCSe)_2]$ (**B**), $[Fe^{II}(L^{S})_2(NCBH_3)_2] \cdot H_2O$ (**C**·H_2O) [L^{S} = 2,5-di(2-pyridyl)-1,3,4-thiadiazole], and $[Fe^{II}(L^{Se})_2(NCS)_2]$ (**2**) (Scheme 2), has been considered for further studies of their magnetic properties.

Description of the Crystal Structures. The molecular structures of $[Fe^{II}(L^{O})_2(NCS)_2]$ (**1**) and $[Fe^{II}(L^{Se})_2(NCS)_2] \cdot 1.4DCM \cdot 0.6MeOH$ (**2**·1.4DCM·0.6MeOH) resemble those of the previously reported 2:1-type complexes $[Fe^{II}(L^{S})_2(NCS)_2]$ (**A**), $[Fe^{II}(L^{S})_2(NCSe)_2] \cdot 1.5DCM \cdot 1.5H_2O$ (**B**·1.5DCM·1.5H_2O),[2] and $[Fe^{II}(L^{S})_2(NCBH_3)_2] \cdot DCM \cdot H_2O$ (**C**·DCM·H_2O).[2] The bidentate chelating ligand coordinates equatorially to the iron(II) ion, leading to a $(N',N^1)_2$-coordination. Trans-coordination of the coligands NCX^- (X = S, Se or BH_3) results in a distorted octahedral N_6 coordination sphere. Both configurations of **1** crystallize in the monoclinic space group $P_2(1)/n$, whereas **2**·1.4DCM·0.6MeOH crystallizes in the triclinic space group $\bar{P}1$. The asymmetric units each consist of one ligand molecule, one coligand molecule, and one iron(II) metal ion at a special position with 0.5 occupancy—identical to the complexes **B**·1.5DCM·1.5H_2O and **C**·DCM·H_2O of ligand L^{S}.[2] In **2**·1.4DCM·0.6MeOH (as well as in **B**·1.5DCM·1.5H_2O and **C**·DCM·H_2O), additionally disordered solvent molecules exist. The odd one out in this context is the structure of **A**, which consists of two such half complexes in the asymmetric unit.[8] At 100 K, according to single crystal X-ray diffraction analyses, the iron(II) ions of complexes **2**·1.4DCM·0.6MeOH [Fe−N: 1.933(3)−2.022(3) Å] of ligand L^{Se}, **A**,[8] **B**·1.5DCM·1.5H_2O, and **C**·DCM·H_2O[2] of ligand L^{S} reside in the low-spin state, whereas the metal ions of both isomers of **1** [Fe−N: 2.058(1)−2.239(1) Å] of ligand L^{O} remain in the high-spin state. In all complexes but one isomer of **1** the ligands adopt s-trans conformation, also typically observed for L^{S} and similar ligands,[2] where the nitrogen atoms of the pyridine side chains point in opposite directions (Figure S2, Supporting Information). The pyridine rings are aligned with twist angles of 3.9 and 0.7° for **1a** and **2**·1.4DCM·0.6MeOH, respectively. Surprisingly, in the second isomer of **1**, namely **1b**, the ligand adopts the s-cis conformation with a twist angle of 14.8° of the pyridine rings (Figure 2b). In 110 structures of the type $[M(L)_2(L')_2]^{n+}$ (M = transition metal, L = di(2-pyridyl) substituted azole ligand, L′ = coligand] reported to the Cambridge Crystallographic Data Centre[40] only eight structures where identified to adopt this conformation, all of them being derivatives of 1,2,4-triazole.[41−47] As usual for complexes of L^{S},[2,8] the general trend for the distances $Fe-N_{pyr} > Fe-N_{azole} > Fe-N_{NCS}$ is also observed for complexes **1a** and **2**·1.4DCM·0.6MeOH of L^{O} and L^{Se}, respectively, whereas $Fe-N_{pyr}$ [2.218(1) Å] is slightly shorter then $Fe-N_{azole}$ [2.239(1) Å] in **1b**. Table 1 summarizes the crystallographic data of complexes **1a**, **1b**, and **2**·1.4DCM·0.6MeOH. Table S1, Supporting Information, summarizes selected bond distances,

dx.doi.org/10.1021/ic400342m | Inorg. Chem. 2013, 52, 6000−6010

Table 1. Crystallographic Data for L^{Se}, $[Fe^{II}(L^{O})_2(NCS)_2]$ (1a and 1b), and $[Fe^{II}(L^{Se})_2(NCS)_2]\cdot 1.4DCM\cdot 0.6MeOH$ ($2\cdot 1.4DCM\cdot 0.6MeOH$)

	L^{Se}	1a	1b	$2\cdot 1.4DCM\cdot 0.6MeOH$
empirical formula	$C_{12}H_8N_4Se$	$C_{26}H_{16}FeN_{10}O_2S_2$	$C_{26}H_{16}FeN_{10}O_2S_2$	$C_{28}H_{21.2}Cl_{2.8}FeN_{10}O_{0.6}S_2Se_2$
formula weight [g mol^{-1}]	287.18	620.46	620.46	884.50
crystal system	monoclinic	monoclinic	monoclinic	triclinic
space group	$P2(1)/c$	$P2(1)/n$	$P2(1)/n$	$\bar{P}1$
a [Å]	6.3904(2)	8.5536(2)	9.5518(2)	7.5704(2)
b [Å]	15.6912(4)	12.0791(3)	7.7916(2)	9.2523(3)
c [Å]	11.2513(3)	13.0494(3)	17.7393(3)	12.5256(4)
α [deg]	90	90	90	90.506(2)
β [deg]	101.1460(10)	92.084(2)	95.8981(11)	105.465(2)
γ [deg]	90	90	90	103.219(2)
V [Å^3]	1106.92(5)	1347.37(6)	1313.24(5)	820.89(4)
Z	4	2	2	1
ρ_{calcd} [g cm^{-3}]	1.723	1.529	1.569	1.789
μ [mm^{-1}]	3.372	0.761	0.780	3.073
temperature [K]	100(2)	100(2)	100(2)	100(2)
$F(000)$	568	632	632	438
crystal color and shape	colorless block	red block	red block	green block
crystal size [mm^3]	0.20 × 0.17 × 0.10	0.09 × 0.03 × 0.03	0.10 × 0.06 × 0.02	0.10 × 0.05 × 0.03
$\theta_{min}/\theta_{max}$ [deg]	2.26/33.13	2.80/26.28	2.31/34.85	2.27/28.28
h	−9 → 9	−10 → 10	−15 → 15	−10 → 10
k	−24 → 24	−15 → 13	−12 → 12	−12 → 12
l	−15 → 17	−16 → 16	−23 → 27	−16 → 16
reflections collected	17434	18142	20856	18189
independent reflections	4214 [R_{int} = 0.0214]	2729 [R_{int} = 0.0486]	5417 [R_{int} = 0.0302]	4056 [R_{int} = 0.0583]
completeness to θ_{max} [%]	99.9	100.0	94.6	99.7
data/restraints/parameters	4214/0/154	2729/0/187	5417/0/187	4056/6/243
GOOF	1.062	1.012	1.048	1.016
$R1/wR2$ [$I > 2\sigma(I)$][a]	0.0214/0525	0.0345/0.0768	0.0347/0.0813	0.0407/0.0908
$R1/wR2$ (all data)[a]	0.0269/0.0543	0.0561/0.0857	0.0499/0.0877	0.0602/0.0986
max peak/hole [e Å^{-3}]	0.503/−0.276	0.291/−0.356	0.596/−0.416	0.832/−1.004

[a] $R1 = \sum[|F_0| - |F_c|]/\sum|F_0|$; $wR2 = (\sum[w(F_0^2 - F_c^2)^2]/\sum[w(F_0^2)^2])^{1/2}$; $w = [\sigma_c^2(F_0^2) + (xP)^2 + yP]^{-1}$; $P = (F_0^2 + 2F_c^2)/3$.

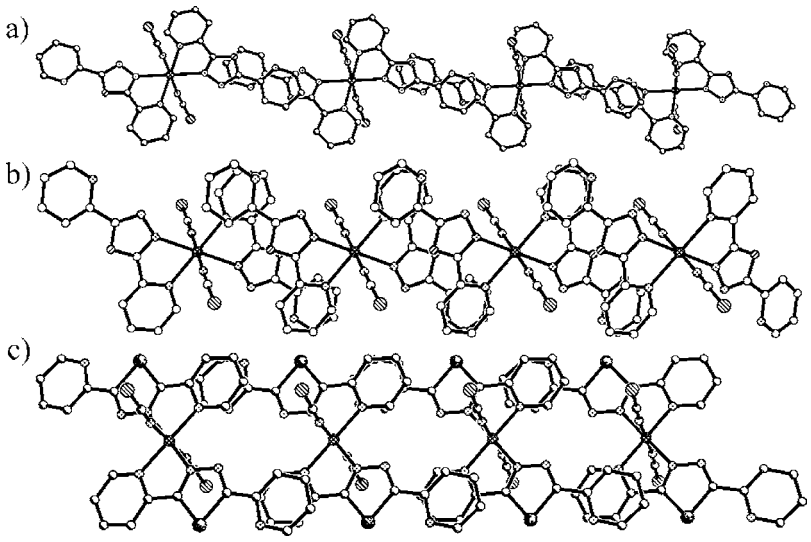

Figure 3. Top views of the chains in the crystal structures of (a) $[Fe^{II}(L^{O})_2(NCS)_2]$ (**1a**); (b) $[Fe^{II}(L^{O})_2(NCS)_2]$ (**1b**); (c) $[Fe^{II}(L^{Se})_2(NCS)_2]\cdot 1.4DCM\cdot 0.6MeOH$ ($2\cdot 1.4DCM\cdot 0.6MeOH$). Hydrogen atoms and solvent molecules have been omitted for clarity.

angles, and geometrical parameters of the coordination spheres. As observed in the related complexes $[Fe^{II}(\mathbf{abpt})_2(NCS)_2]$ and $[Fe^{II}(\mathbf{abpt})_2(NCSe)_2]$ [**abpt** = 4-amino-3,5-di(2-pyridyl)-4*H*-1,2,4-triazole][48] both isomers of complex **1** also pack in linear chains where overlapping ligands form chains that run roughly parallel to the coordination vectors (Figure 3a and b). But unlike the former two complexes, where close packing is achieved by $\pi-\pi$-interactions, in **1a** and **1b**, neighboring ligands are separated with shortest centroid-{O(1)/C(6)/N(2)/N(3)/C(7)}···centroid-{C(8)−C(12)/N(4)} and centroid-{C(1)−

dx.doi.org/10.1021/ic400342m | Inorg. Chem. 2013, 52, 6000−6010

C(5)/N(1)}···centroid-{C(8)−C(12)/N(4)} distances of 4.03 and 4.23 Å, respectively. The situation in **2**·1.4DCM·0.6MeOH is slightly different and similar to that in complexes **A**, **B**·1.5DCM·1.5H_2O, and **C**·DCM·H_2O,[2] where chains are made up of complex units which stack perpendicularly to the coordination vectors (Figure 3c). In **2**·1.4DCM·0.6MeOH, a centroid-{C(1)−C(5)/N(1)}···centroid-{C(8)−C(12)/N(4)} distance of 3.95 Å is observed.

In all complexes included in this study only few weak short contacts with atom distances less than the Van-der-Waals (VdW) radii < 0.05 Å are observed (Table S2, Supporting Information). No significant classical hydrogen bonds, $\pi-\pi$-interactions, or similar relatively strong intermolecular interactions are observed. However, in the selenadiazole complex **2**·1.4DCM·0.6MeOH a Se···S distance [Se(1)···S(50) 3.745 Å] only insignificantly longer than the sum of VdW-radii has been observed between the selenadiazole ring and the coligand of a neighboring complex molecule. For complex **A** with two independent SCO molecules within the asymmetric unit similarly weak S···S interactions are observed at 100 K. Here, coligand sulfur atoms of the two distinct molecules are slightly farther apart than the sum of VdW-radii. However, at 140 K and RT, the respective distance increases significantly (Table S2, Supporting Information). If solvent molecules are present in the packing, they are disordered and/or not fully occupied. Therefore short contacts involving them are to be regarded warily. Additionally, in those cases the composition of the bulk material unfortunately varies from that of the crystal structure, usually by loss of solvent molecules. Therefore short contacts between complex and solvent molecules have not been considered in this discussion, although they have been included in Table S2 (Supporting Information).

Magnetic Properties. Recently, complexes $[Fe^{II}(L^S)_2(NCS)_2]$ (**A**),[2,8] $[Fe^{II}(L^S)_2(NCSe)_2]$ (**B**),[2] and $[Fe^{II}(L^S)_2(NCBH_3)_2]\cdot H_2O$ (**C**·H_2O)[2] of L^S have been reported as SCO complexes featuring two SCO steps at $T_{1/2}$ = 112 and 167 K (**A**)[8] and one SCO step at $T_{1/2}$ = 192 (**B**) and 285 K (**C**·H_2O) (Figure 4).[2] In this study, the variable-temperature magnetic properties of complexes **1** and **2**·MeOH have been studied, as have been the reflectivity and photomagnetic properties of the series **A**, **B**, **C**·H_2O, and **2**·MeOH.

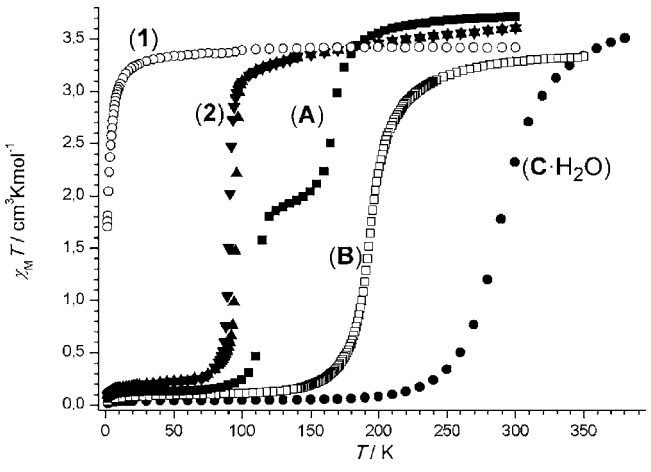

Figure 4. $\chi_M T$ vs T plots for $[Fe^{II}(L^O)_2(NCS)_2]$ (**1**) (open circles, ○), $[Fe^{II}(L^{Se})_2(NCS)_2]\cdot$MeOH (**2**·MeOH) (cooling mode full triangles down, ▼; heating mode full triangles up, ▲), $[Fe^{II}(L^S)_2(NCS)_2]$ (**A**)[8] (full squares, ■), $[Fe^{II}(L^S)_2(NCSe)_2]$ (**B**) (open squares, □), and $[Fe^{II}(L^S)_2(NCBH_3)_2]\cdot H_2O$ (**C**·H_2O) (full circles, ●).[2]

Variable-temperature magnetic susceptibility measurements were carried out on amorphous bulk material of **1**, and on crystalline bulk material formulated as **2**·MeOH over the range 300−2 K (Figure 4). For both samples, the room temperature values $\chi_M T$ = 3.42 and 3.59 cm^3 K mol^{-1} (μ_{eff} = 5.23 and 5.36 μ_B), respectively, compare well to the calculated spin-only values of $\chi_M T$ = 3.00 cm^{3}K mol^{-1} (μ_{eff} = 4.90 μ_B) for one high-spin iron(II) ion. As the temperature is decreased, the $\chi_M T$ value of **1** remains constant down to 30 K before decreasing upon further cooling. The experimental data of **1** was fitted to the Curie−Weiss law $\chi_M = C/(T - \Theta)$ using the parameters C = 3.44 cm^3 K mol^{-1} and Θ = −1.47 K, thus indicating that magnetic interactions between the metal centers are negligible. SCO behavior was not observed. For compound **2**·MeOH however, a dramatic drop of the $\chi_M T$ values to almost zero has been observed around 90 K on lowering the temperature, indicating abrupt SCO behavior (Figure 4). On reheating the compound a small reproducible thermal hysteresis was observed. The SCO temperatures $T_{1/2}(\downarrow)$ = 91 K and $T_{1/2}(\uparrow)$ = 96 K were obtained from the first derivatives of the SCO curves in the cooling and heating mode, respectively (Figure S4, Supporting Information).

Reflectivity Studies. The process of spin crossover of $[Fe^{II}(L^S)_2(NCS)_2]$ (**A**),[2,8] $[Fe^{II}(L^S)_2(NCSe)_2]$ (**B**),[2] $[Fe^{II}(L^S)_2(NCBH_3)_2]\cdot H_2O$ (**C**·H_2O),[2] and $[Fe^{II}(L^{Se})_2(NCS)_2]\cdot$MeOH (**2**·MeOH) was also monitored following the thermal behavior of the respective visible spectra, measured by diffuse reflectance spectroscopy. Figures 5 and S4−S6 show the spectral changes of the compounds as a function of the temperature. The compounds analyzed are very absorbing below ca. 700 nm; therefore changes can best be followed above that wavelength. The spectra are constituted by a main MLCT band in the 500−800 nm region characteristic of the LS species, centered at 600−650 nm with several shoulders at about 700 and 800 nm. This band spreads over the visible range and hides the d−d band of the HS state around 820−860 nm, appearing as shoulder.

Upon cooling compound $[Fe^{II}(L^S)_2(NCS)_2]$ (**A**) to 100 K, the MLCT band observed in the absorption spectra increases, whereas the shoulder at around 860 nm decreases (Figure 5). This indicates the population of the LS state of **A**. The reflectivity signal followed at 800 nm indicates clear two-step SCO behavior of the compound with a large plateau spreading over 160 to 120 K. The thermal spin-crossover temperatures ascertained with this method are 170 and 112 K, in good agreement with the magnetic data.[8] Below 75 K, the absorption spectra behave in the opposite way, as the MLCT strongly decreases inducing an increase of the reflectivity signal at 800 nm. The spectrum at 10 K is similar to the one observed at 280 K, proving the population of the HS state according to the LIESST effect (Figure 5b). Compounds $[Fe^{II}(L^S)_2(NCSe)_2]$ (**B**) of the isoselenocyanate coligand and $[Fe^{II}(L^{Se})_2(NCS)_2]\cdot$MeOH (**2**·MeOH) of the selenodiazole ligand exhibit similar behavior, exposed to identical conditions, except that the two-step character of the spin-crossover is not observed (Figure S5 and S6, Supporting Information). $T_{1/2}$ is estimated to be around 200 and 95 K, respectively, close to the values determined by magnetic investigations.[2]

Below 70 and 75 K, respectively, the reflectivity signals recorded at 750 and 850 nm for **B** (Figure S5, Supporting Information) and 800 nm for **2**·MeOH (Figure S7, Supporting

dx.doi.org/10.1021/ic400342m | Inorg. Chem. 2013, 52, 6000−6010

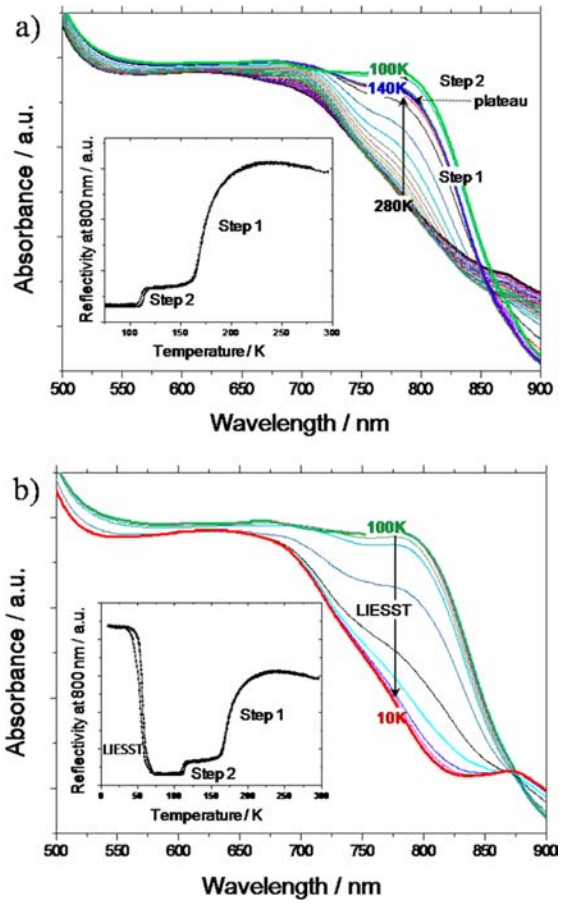

Figure 5. Thermal dependence of the absorption spectrum of $[Fe^{II}(L^S)_2(NCS)_2]$ (**A**) (a) from room temperature to 100 K and (b) from 100 to 10 K. The insets report the reflectivity signal followed at 800 nm upon thermal variations.

Information) indicate the occurrence of the LIESST effect for those compounds. The spectra at 10 K are similar to the ones recorded at RT, proving the population of the HS state. A slight hysteresis recorded under light irradiation of **2**·MeOH (Figure S7, inset) corresponds to light induced thermal hysteresis (LITH) at low temperature. This may indicate that also for the photoinduced process, cooperative interactions are not negligible. This is further confirmed by the kinetics which follow sigmoidal behavior, typical of cooperative networks (see below). Under identical reaction conditions a gradual spin crossover is observed for the cyanoborohydride complex $[Fe^{II}(L^S)_2(NCBH_3)_2]\cdot H_2O$ (**C**·H_2O). From 200−290 K, the reflectivity signal strongly increases but does not saturate, suggesting that the spin crossover is not complete. Therefore, $T_{1/2}$ cannot be properly estimated. This is also in agreement with the magnetic data which reported $T_{1/2}$ = 285 K.[2] Concerning the low temperature behavior of this compound, the absorption spectra do not change upon cooling, and the reflectivity signal at 800 nm remains constant. This indicates that no LIESST effect occurs at the surface of the sample (Figure S6, Supporting Information).

Photomagnetic Properties. Regarding the results of the reflectivity measurements, the photomagnetic properties of all SCO compounds of the examined series were investigated. Irradiation was tested on samples **A**, **B**, **C**·H_2O, and **2**·MeOH at different wavelengths. Only the cyanoborohydride compound **C**·H_2O did not exhibit any photomagnetic properties. Whatever the wavelength and the power of irradiation, no changes in the magnetic signal have been observed. Concerning **A**, **B**, and **2**·MeOH, the best conditions to record the T(LIESST) curves were found to be at 647 nm with a 5 mW/cm^2 power (Figure 6). In all cases, a quantitative photoconversion was observed. After photosaturation was reached, the light was switched off and the T(LIESST) curves were recorded.[13,16,49]

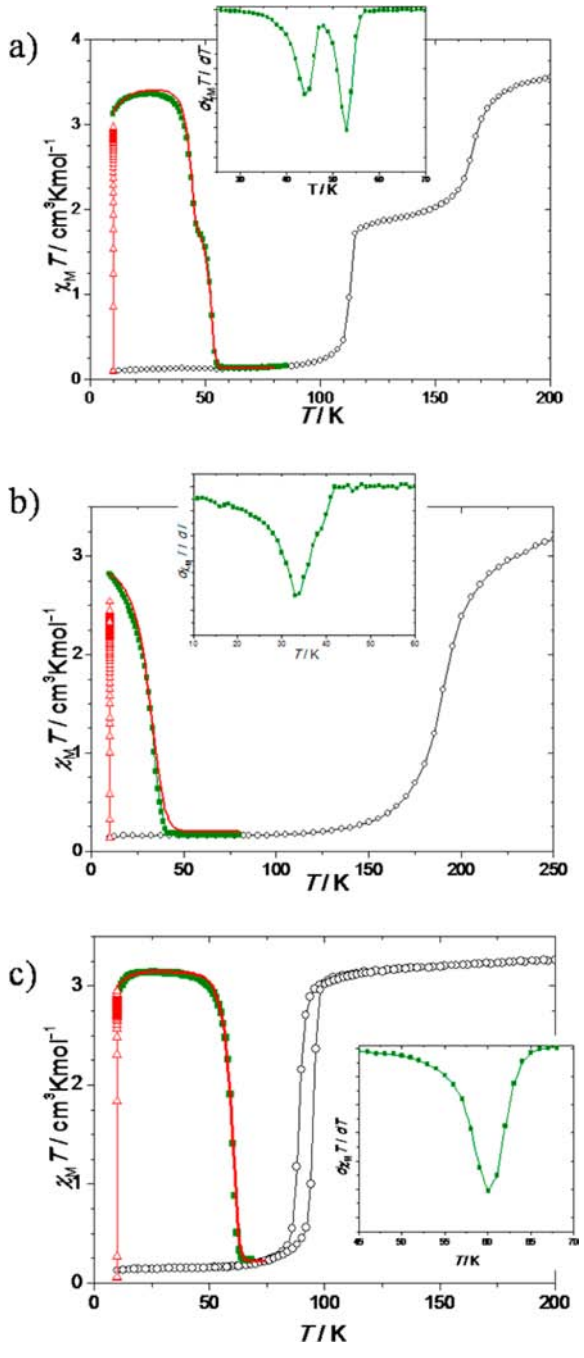

Figure 6. Thermal behavior of $\chi_M T$ before irradiation (open circles, ○), during irradiation (open triangles up, △), and in the dark after irradiation (full squares, ■). (inset) First derivative of the $\chi_M T$ vs T curve recorded in the dark after irradiation whose minimum gives access to the T(LIESST) value. The full red lines stand for the T(LIESST) simulation performed as discussed in the text: (a) $[Fe^{II}(L^S)_2(NCS)_2]$ (**A**); (b) $[Fe^{II}(L^S)_2(NCSe)_2]$ (**B**); (c) $[Fe^{II}(L^{Se})_2(NCS)_2]\cdot$MeOH (**2**·MeOH).

dx.doi.org/10.1021/ic400342m | Inorg. Chem. 2013, 52, 6000−6010

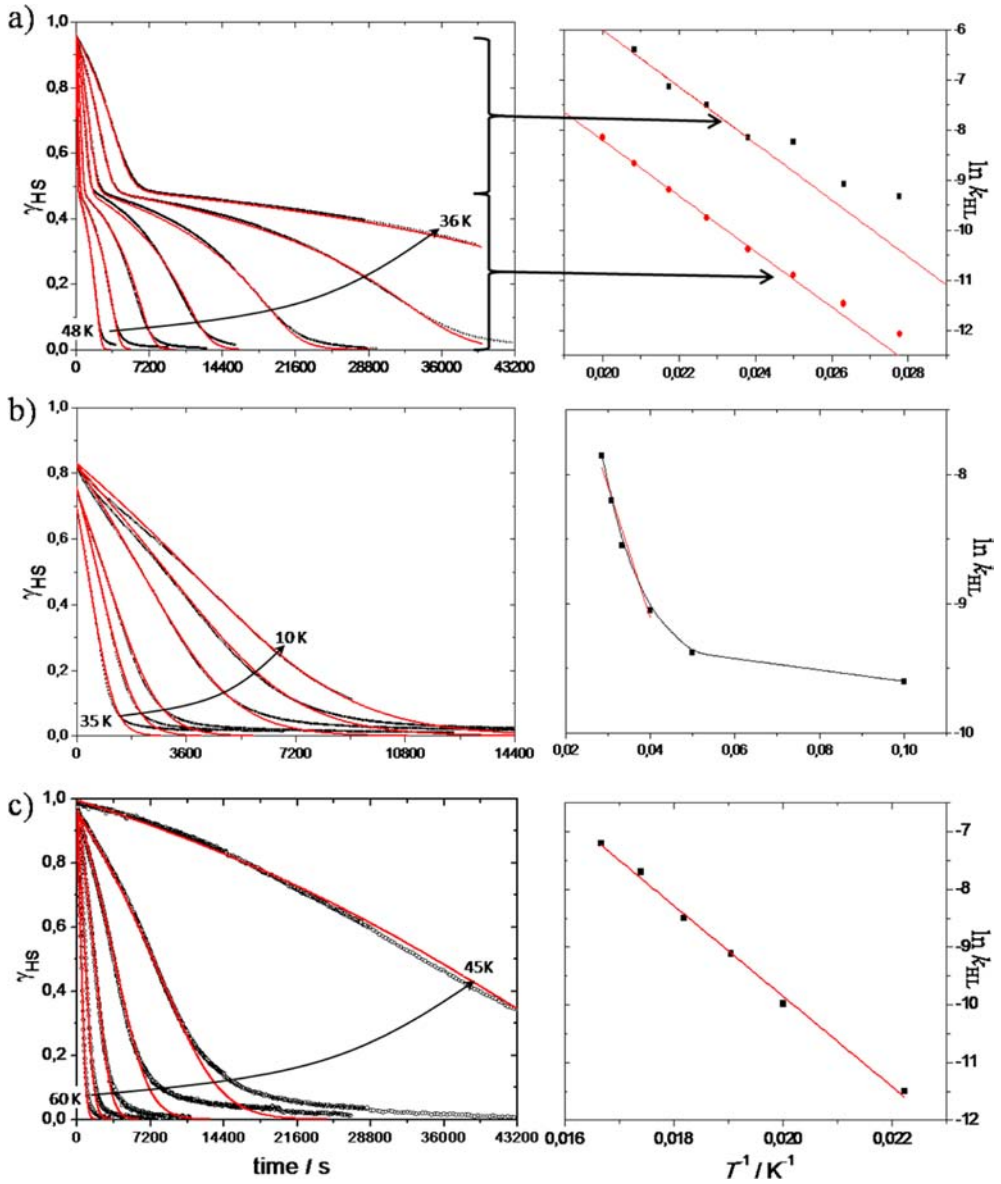

Figure 7. Plots of the different relaxation kinetics recorded as function of the temperature T (a) $[Fe^{II}(\mathbf{L}^{S})_2(NCS)_2]$ (**A**) at 48, 46, 44, 42, 40, 38, and 36 K; (b) $[Fe^{II}(\mathbf{L}^{S})_2(NCSe)_2]$ (**B**) at 35, 30, 25, 20, 15, and 10 K; and (c) $[Fe^{II}(\mathbf{L}^{Se})_2(NCS)_2]$·MeOH (**2**·MeOH) at 60, 57, 54, 51, 48, and 45 K (left) and the corresponding Arrhenius plots (right). The red lines stand for the fits discussed in the main text.

The increase of $\chi_M T$ from 10−30 K observed for **A** and **2**·MeOH after light irradiation is attributed to iron(II) zero-field splitting. For **B**, instead of this increase a decrease of $\chi_M T$ is recorded probably due to a more efficient HS → LS relaxation. For the three compounds **A**, **B**, and **2**·MeOH, the maximum $\chi_M T$ values indicate photoconversion efficiencies of 92, 85, and 100%, respectively. Above 40 K the HS → LS relaxation becomes efficient in **B** and **2**·MeOH and $\chi_M T$ decreases rapidly to reach the baseline above 60 K. From the first derivative of the $\chi_M T$ vs T curves the T(LIESST) values can be extracted (insets Figure 6) leading to values of T(LIESST) = 34 and 60 K, respectively. Concerning **A**, the T(LIESST) curve exhibits a two-step character that reflects nicely the two-step character of the thermal SCO. The presence of the plateau in the thermal spin transition has been explained by the presence of two independent molecules in the asymmetric unit leading to SCO behavior of [HS] + [HS] → [HS] + [LS] → [LS] + [LS]. The step of the T(LIESST) curve is observed at the same $\chi_M T$ value than the plateau in the thermal spin transition, which favors the presence of a similar intermediate [HS] + [LS] phase in the T(LIESST) relaxation curve. The corresponding T(LIESST) values are 44 and 53 K. The presence of such an intermediate state in the T(LIESST) curve of $[Fe^{II}(\mathbf{L}^{S})_2(NCS)_2]$ (**A**) raises the question of its observation during the photo excitation process.

The record of the photoexcitation curve at 10 K under low excitation power shows a continuous increase of the $\chi_M T$ value upon irradiation time. No step or inflection point could be evidenced from this experiment, indicating that irradiation converts the LS state directly into a HS state, similarly as reported for dinuclear compounds of 2,2′-bipyrimidine[27] and recently for a mononuclear compound of 6,6′-bis(amino-2-pyridyl)-2,2′-bipyridine.[50] Several relaxation kinetics have been recorded to characterize the relaxation process of **A**, **B**, and **2**·MeOH (Figure 6).

dx.doi.org/10.1021/ic400342m | Inorg. Chem. 2013, 52, 6000−6010

Table 2. Parameters for Thermal and Light-Induced Spin Transitions Extracted from the Relaxation/T(LIESST) Simulation

compound	$T_{1/2}$ [K]	T(LIESST) [K]	E_a [cm^{-1}]	E_a^* [cm^{-1}]	k_0 [s^{-1}]	k_∞ [s^{-1}]
A (step 1)	167	44	390/380	85/85	$8 \times 10^{-5}/3 \times 10^{-5}$	200/250
A (step 2)	112	53	420/420	110/110	$5 \times 10^{-6}/3 \times 10^{-6}$	10/17
B	192	34	70/65	40/45	$5 \times 10^{-5}/6 \times 10^{-5}$	$6.5 \times 10^{-3}/7.5 \times 10^{-3}$
2·MeOH	93	60	545/535	80/90	$1 \times 10^{-5}/1 \times 10^{-5}$	350/360

Relaxation Kinetics. Compound **A** clearly exhibits two-step relaxation behavior as expected from the T(LIESST) curve shape. Both steps exhibit a sigmoidal shape. If the relaxation process is [HS−HS] → [HS−LS] → [LS−LS], as in dinuclear systems,[26,27] where the second relaxation step depends on the lifetime of the first one, the relaxation kinetics should account for this dependence. On the other hand, if the relaxation processes are due to two independent metastable sites, the two relaxation rates are not correlated.[30,31] This latter situation is appropriate to describe the behavior of the two-step SCO complex **A**, especially because the two relaxation processes have sufficiently different time scales to be treated separately.

We have considered a sigmoidal law to describe the photoinduced HS decay of each site of **A**:

$$\frac{d\gamma_{HS1}}{dt} = -k(T)e^{\alpha 1(T)(1-\gamma_{HS1})}\gamma_{HS1}$$

and

$$\frac{d\gamma_{HS2}}{dt} = -k(T)e^{\alpha 2(T)(1-\gamma_{HS2})}\gamma_{HS2}$$

with $\alpha = E_a^*/k_BT$ being the additional activation energy due to the cooperativity present in the material and the global behavior $\gamma_{HS} = a\gamma_{HS2} + b\gamma_{HS1}$ with $a = b = 1/2$. The results of the simulation procedure are shown in Figure 7a. Quite nice agreements between experiment and simulation could be obtained leading to the parameters extracted from the Arrhenius plot (Figure 7a) and summarized in Table 2. From these simulations, the Arrhenius plot could be drawn for each site giving rise to quite close sets of parameters. However, this difference is sufficient to lead to nicely observable two-step relaxation and T(LIESST) curves.

Regarding compounds **B** and **2**·MeOH, a classical sigmoidal law with only one relaxation rate, was used to reproduce the experimental behavior.

$$\frac{d\gamma_{HS}}{dt} = -k(T)e^{\alpha(T)(1-\gamma_{HS})}\gamma_{HS}$$

The agreement between simulations and experiments is quite nice. In accordance to its relatively abrupt SCO, the HS → LS relaxation of compound **2**·MeOH clearly follows a self-acceleration process due to cooperative interactions. Also, the contribution of intermolecular cooperativity in **B** is clearly non-negligible on the relaxation kinetics. The only deviation between the simulated and the experimental curves occurs at long time for both compounds, suggesting the presence of some distribution of the activation energy. Concerning the $\ln(k_{HL})$ vs $1/T$ plot, a strong deviation from linearity is observed for compound **B** (Figure 7b), whereas compound **2**·MeOH follows the linearity quite nicely (Figure 7c). Such deviation from linearity, as observed in compound **B**, is typically due to the crossing between the low temperature process where the relaxation is governed by quantum tunnelling and therefore independent of the temperature and the high temperature region where the relaxation is thermally activated.

An elegant way to test the validity of the dynamical parameters obtained from the relaxation kinetics is to use them to simulate the T(LIESST) curves.[15] Whereas for **B** and **2**·MeOH only one site has been considered that led to nice simulated, a two-site model was used for **A** (Figure 6). The agreement between the experiment and the simulation is very nice for **A** giving credit to the model used and parameters extracted.

CONCLUSIONS

The new ligand $\mathbf{L}^{Se}$ has been synthesized, characterized, and used for complexation reactions with iron(II) ions. Also, the first iron(II) complex of $\mathbf{L}^{O}$ has been prepared. With those two ligands, two new complexes belonging to the complex family $[Fe^{II}(\mathbf{L})_2(NCX)_2]$, where **L** is a bidentate chelating ligand and X = S, Se, BH_3, have been synthesized and magnetically characterized. No thermal SCO has been observed on the oxadiazole-compound $[Fe^{II}(\mathbf{L}^{O})_2(NCS)_2]$ (**1**), which remains in the HS state in the temperature range measured. The selenadiazole-compound $[Fe^{II}(\mathbf{L}^{Se})_2(NCS)_2]$·MeOH (**2**·MeOH), however, exhibits a thermal SCO [$T_{1/2}(\downarrow)$ = 91 K, $T_{1/2}(\uparrow)$ = 96 K] with a distinct hysteresis of about 5 K width. In the crystal packing of this compound no strong intermolecular short contact was identified. However, a short Se···S contact insignificantly longer than the sum of vdW radii could be responsible for the hysteresis effect. For further LIESST and photomagnetic studies, four compounds belonging to this family with chalcadiazole ligands, namely $[Fe^{II}(\mathbf{L}^{S})_2(NCS)_2]$ (**A**),[2,8] $[Fe^{II}(\mathbf{L}^{S})_2(NCSe)_2]$ (**B**), $[Fe^{II}(\mathbf{L}^{S})_2(NCBH_3)_2]$ (**C**),[2] and $[Fe^{II}(\mathbf{L}^{Se})_2(NCS)_2]$·MeOH (**2**·MeOH), have been considered. Anionic coligands NCX (X = S, Se, BH_3) coordinate trans to the metal ions. Changing those coligands from NCS^-, to $NCSe^-$ and $NCBH_3^-$, the thermal spin-crossover temperature $T_{1/2}$ is increased whereas T(LIESST) is decreased and even absent in the $NCBH_3$-derivative. In addition, concerning the particular case of the NCS-derivative **A** of $\mathbf{L}^{S}$, the two-step character of the thermal spin-crossover is nicely reflected in the T(LIESST) curve and the relaxation kinetics. The cooperative behavior of each step expresses itself in sigmoidal behavior of the isothermal HS fraction decay. The behavior has been reproduced accounting for two independent relaxing sites. According to the inverse energy gap law[51,52] and the T(LIESST) vs $T_{1/2}$ database,[14,15] the lowest T(LIESST) value was linked to the high temperature thermal spin crossover ($T_{1/2}$ = 167 K) whereas the highest T(LIESST) corresponds to the $T_{1/2}$ = 112 K conversion. Considering the four [T(LIESST), $T_{1/2}$] values of the NCS^- and $NCSe^-$ derivatives **A**, **B**, and **2**·MeOH, according to the database proposed by Létard et al., all belong to the T_0 = 90 K line with T(LIESST) = $T_0 - 0.3T_{1/2}$ (Figure 1).[14] Extrapolation to the $T_{1/2}$ value of 285 K of the cyanoborohydride compound **C**·H_2O of $\mathbf{L}^{S}$, T(LIESST) is estimated to be around 5 K, a value not recordable with a SQUID magnetometer, in agreement

dx.doi.org/10.1021/ic400342m | Inorg. Chem. 2013, 52, 6000−6010

with our experimental investigation which does not allow detection of LIESST properties.

EXPERIMENTAL SECTION

All starting materials and metal salts were purchased from Sigma-Aldrich and used as received. All solvents used were laboratory reagent grade. If not stated otherwise, manipulations were carried out in air. Melting points were determined using a Thiele melting point apparatus. Elemental analyses were carried out at the Karlsruhe Institute for Technologie with an Elementar Vario Micro Cube. IR spectra were recorded over the range 4000−400 cm^{-1} using a Nicolet Magna 760 FTIR spectrometer. Variable-temperature magnetic susceptibility measurements were carried out on amorphous samples (**1**) or microcrystalline, ground samples (**2**·MeOH) using a Quantum Design MPMSXL SQUID susceptometer over the range 300−2 K (0.1 T) in both the cooling and heating mode. Reflectivity measurements were performed using a custom-built setup equipped with a SM240 spectrometer (Opton Laser International). This equipment allows recording both the diffuse absorption spectra within the range of 500−900 nm at a given temperature and the temperature dependence (10−290 K) of the reflectivity signal at a selected wavelength (±2.5 nm). Photomagnetic measurements were performed using a Spectrum Physics Series 2025 Kr^+ laser (514.5 or 676 nm at 5 mw/cm^2) or a 830 nm photodiode (3.5 mW/cm^2), coupled by means of an optical fiber to the cavity of a MPMS-5S Quantum Design SQUID magnetometer. The optical power at the sample surface was adjusted to prevent warming of the sample. The compounds consist of a solid thin layer. Its weight was obtained by comparison of the thermal spin-crossover curve with that of a more accurately weighted sample of the same material. A standardized method for measuring LIESST data, published previously,[49] was followed: After being slowly cooled to 10 K, the sample in the low-spin state was irradiated and the change in magnetic susceptibility was followed. When the saturation point was reached the laser was switched off and the temperature increased at a rate of ≈0.3 K min^{-1}. The magnetization was measured every 1 K. T(LIESST) was determined from the minimum of a $d\chi_M T/dT$ vs T plot for the relaxation process. Single crystal X-ray diffraction data were collected using a Rigaku R-AXIS Spider IP area detector diffractometer or a Bruker APEX-II CCD diffractometer with a microfused sealed tube radiation source, using graphite-monochromated Mo Kα radiation (λ = 0.71073 Å). The structures were solved by direct methods with SHELXS-97[53] and refined against F^2 using all data by full-matrix least-squares techniques with SHELXL-97.[53] All non-hydrogen atoms were refined anisotropically. All hydrogen atoms were placed at calculated positions using riding models. In **2**·1.4DCM·0.6MeOH, partially occupied DCM solvate molecule share the approximate positions with partially occupied MeOH solvate molecules, adding up to a sum of 1.0 for the asymmetric unit. The partially occupied MeOH solvates were located from the difference maps and fixed at the respective positions. Orientations of non-coordinating pyridine rings were determined as follows. The remaining maximum electron densities, after all non-hydrogen atoms have been refined, unambiguously revealed the positions of all hydrogen atoms—including the one in question [H(9)]—allowing the differentiation of "N" and "C−H". Additionally all structures in question have tentatively been refined with reversed pyridine rings, which resulted in considerably poorer final parameters in all cases. CCDC 905996-905999 contains the supplementary crystallographic data for the structures reported in this article. These data can be obtained free of charge at www.ccdc.cam.ac.uk/data_request/cif or from the Cambridge Crystallographic Data Centre, 12 Union Road, Cambridge CB2 1EZ, UK.

2,5-Di(2-pyridyl)-1,3,4-oxadiazole (L^O). 2-Cyanopyridine (20.0 mL, 21.6 g, 207 mmol) was added to hydrazine monohydrate (20.1 mL, 20.7 g, 414 mmol). The resulting mixture was warmed in a water bath for 3 h. During that time, the reaction mixture solidified completely, was collected, and crystallized from pyridine to yield 3,6-di(2-pyridy1)-1,2-dihydro-1,2,4,5-tetrazine (**III**) as orange needles. The product was used as such. Dihydrotetrazine **III** (13.4 g, 56.2 mmol) was dissolved in hot aqueous hydrochloric acid (120 mL, 2.5 N). The solution was cooled to 0 °C, and a solution of sodium nitrite (11.0 g, 0.16 mol) in H_2O (50 mL) was added over 1.5 h. During that time heavy effervescence and a color change from amber to pink was observed. The reaction mixture was boiled until it turned nearly colorless, concentrated under reduced pressure, and made alkaline with concentrated NaOH solution. After extraction with Et_2O (3 × 50 mL), the combined organic layers were dried over Na_2SO_4 and all volatiles were removed under reduced pressure. Recrystallization with EA yielded the title compound as a beige solid. Yield 41%. IR (diamond ATR): $\tilde{\nu}$ = 3096.6, 3084.2, 3058.5, 3019.6, 2992.5, 1588.3 (s), 1570.1, 1554.7, 1548.2, 1451.2 (vs), 1436.0 (s), 1413.3, 1306.8, 1288.4, 1278.9, 1249.6, 1157.5, 1144.0, 1095.2 (s), 1048.2, 994.7, 971.0, 896.9, 866.0, 798.2, 741.4 (s), 727.1, 714.4 (s), 620.0, 529.1, 402.2 cm^{-1} (literatrure ref 54). ^{1}H NMR (400.17 MHz, DMSO-d_6): δ = 8.83 (ddd, $^3J_{5,6}$ = 4.8, $^4J_{4,6}$ = 1.7, $^5J_{3,6}$ = 1.0 Hz, 2 H, 6-Py*H*), 8.29 (td, $^3J_{3,4}$ = 7.8, $^4J_{3,5}$ = $^5J_{3,6}$ = 1.0 Hz, 2 H, 3-Py*H*), 8.09 (dt, $^3J_{3,4}$ = $^3J_{4,5}$ = 7.8, $^4J_{4,6}$ = 1.7 Hz, 2 H, 4-Py*H*), 7.68 (ddd, $^3J_{4,5}$ = 7.8, $^3J_{5,6}$ = 4.8, $^4J_{3,5}$ = 1.0 Hz, 2 H, 5-Py*H*) ppm (literature ref 55). ^{13}C NMR (100.62 MHz, DMSO-d_6): δ = 164.4 (Az*C*), 150.8 (6-Py*C*), 142.8 (2-Py*C*), 138.3 (4-Py*C*), 127.1 (5-Py*C*), 123.7 (3-Py*C*) ppm.

2,5-Di(2-pyridyl)-1,3,4-selenadiazole (L^{Se}). Under inert conditions, Woollins' reagent (573 mg, 1.07 mmol) was added to toluene (dry, 25 mL). To the resulting suspension a suspension of *N*′-picolinoylpicolinohydrazide (260.9 mg, 1.07 mmol) in toluene (dry, 10 mL) was added. This mixture was refluxed for 24 h, turning to an orange solution. After all volatiles were reduced, the residue was purified by column chromatography (silica gel) using DCM/EA (5:1) as eluent under argon pressure. Yield: 24%. Elemental analysis (%) found: C 49.99, H 2.94, N 19.10; calcd. for $C_{12}H_8N_4Se$ (287.18 g mol^{-1}: C 50.19, H 2.81, N 19.51. IR (diamond ATR): $\tilde{\nu}$ = 3089.1, 3057.2, 2961.6, 2921.9, 1581.5 (s), 1565.9, 1484.8, 1443.7, 1423.4 (vs), 1300.8, 1274.0, 1260.7, 1244.0, 1216.2, 1145.7, 1089.9, 1067.6, 1047.6, 999.1 (vs), 960.4, 919.9, 891.8, 788.8 (s), 778.3 (vs), 747.6, 738.0 (s), 684.4 (s), 614.6 (s), 582.0 (vs), 544.9, 519.9, 465.7, 407.9 cm^{-1}. ^{1}H NMR (200.13 MHz, $CDCl_3$): δ = 8.65 (ddd, $^3J_{5,6}$ = 4.8, $^4J_{4,6}$ = 1.7, $^5J_{3,6}$ = 1.0 Hz, 2 H, 6-Py*H*), 8.36 (td, $^3J_{3,4}$ = 7.7 Hz, $^4J_{3,5}$ = $^5J_{3,6}$ = 1.0 Hz, 2 H, 3-Py*H*), 7.85 (dt, $^3J_{3,4}$ = $^3J_{4,5}$ = 7.7, $^4J_{4,6}$ = 1.7 Hz, 2 H, 4-Py*H*), 7.39 (ddd, $^3J_{4,5}$ = 7.7, $^3J_{5,6}$ = 4.8, $^4J_{3,5}$ = 1.0 Hz, 2 H, 5-Py*H*) ppm. ^{13}C NMR (100.62 MHz, $CDCl_3$): δ = 179.3 (Az*C*), 151.7 (2-Py*C*), 150.2 (6-Py*C*), 137.1 (4-Py*C*), 125.3 (5-Py*C*), 120.2 (3-Py*C*) ppm.

$[Fe^{II}(L^O)_2(NCS)_2]$ (1). In an argon atmosphere, a solution of KSCN (29.2 mg, 300 μmol) in MeOH (5 mL) was added to a solution of $FeSO_4$·$7H_2O$ (41.7 mg, 150 μmol) in MeOH (5 mL). The resulting suspension was stirred for 1 h before the solvent was removed under reduced pressure. The residue was triturated with MeOH (3 mL), and the resulting suspension was filtered. A clear solution of "$Fe(NCS)_2$" was obtained. To this solution was added a solution of L^O (67.3 mg, 300 μmol) in MeOH (3 mL). The resulting mixture was left for stirring at RT overnight. Filtration and drying in vacuo gave amorphous bulk of $[Fe(L^O)_2(NCS)_2]$ (**1**). Yield 45%. Elemental analysis (%) found: C 49.61, H 2.60, N 22.48, S 10.26; calcd for $C_{26}H_{16}N_{10}O_2S_2Fe$ (620.45 g mol^{-1}): C 50.33, H 2.60, N 22.58, S 10.33. IR (diamond ATR): $\tilde{\nu}$ = 2067.4 (vs), 1614.6, 1586.6, 1571.7, 1544.1, 1479.2, 1458.6, 1441.2 (s), 1392.8, 1313.6, 1296.0, 1254.8, 1157.0, 1091.5 (s), 1043.1, 1012.9, 994.2, 959.8, 906.6, 796.8 (s), 742.3, 732.8, 711.6 (s), 636.9, 619.3, 541.4, 470.9, 439.2, 411.9 cm^{-1}. HR ESI-MS (MeCN): m/z = 562.050 $[Fe(L^O)_2(NCS)]^+$, 379.006 $[Fe(L^O)(NCS)(MeCN)]^+$, 225.077 $[HL^O]^+$. Single crystals of complex $[Fe(L^O)_2(NCS)_2]$ (**1**) as a mixture of **1a** and **1b** suitable for X-ray diffraction studies were obtained by carefully layering ligand and metal salt solutions in MeOH.

$[Fe^{II}(L^{Se})_2(NCS)_2]$ (2). In an argon atmosphere a freshly prepared solution of $Fe(SCN)_2$ (150 μmol) in MeOH (2 mL) was layered with a solution of L^{Se} (86.15 mg, 300 μmol) in DCM (2 mL). Overnight, a dark green crystalline solid formed. Filtration and drying in vacuo gave bulk of $[Fe^{II}(L^{Se})_2(NCS)_2]$·MeOH (**2**·MeOH). Yield 77%. Elemental analysis (%) found: C 41,37, H 2,25, N 17,64, S 8.20; calcd for $C_{27}H_{20}N_{10}OS_2Se_2Fe$ (778.41 g mol^{-1}): C 41.54, H 2.58, N 17.96, S

dx.doi.org/10.1021/ic400342m | *Inorg. Chem.* 2013, 52, 6000−6010

8.35. IR (diamond ATR): $\tilde{\nu}$ = 2073.2 (vs), 2029.4, 2015.0, 1595.4, 1567.3, 1472.8, 1445.0, 1433.2 (s), 1308.0, 1298.1, 1284.0, 1246.9, 1163.5, 1091.5, 1046.8, 1017.8, 994.8, 980.3, 781.1 (vs), 741.7, 693.4, 637.2, 583.7 (s), 556.0, 473.3, 401.1 cm^{-1}. HR ESI-MS (MeCN): m/z = 689.893 $[Fe(L^{Se})(NCS)]^+$, 442.928 $[Fe(L^{Se})(NCS)(MeCN)]^+$, 288.999 $[HL^{Se}]^+$. Green single crystals of $[Fe^{II}(L^{Se})_2(NCS)_2]$·1.4DCM·0.6MeOH (**2**·1.4DCM·0.6MeOH) suitable for X-ray diffraction were obtained by this method.

■ ASSOCIATED CONTENT

Supporting Information

This material is available free of charge via the Internet at http://pubs.acs.org.

■ AUTHOR INFORMATION

Corresponding Author

*Phone: +49-(0)761-203-6135. Fax: +49-(0)761-203-6001. E-mail address: julia.klingele@ac.uni-freiburg.de.

Notes

The authors declare no competing financial interest.

■ ACKNOWLEDGMENTS

This project is supported by the European Social Fund and by the Ministry Of Science, Research and the Arts Baden-Württemberg within the *Margarete von Wrangell Program*. J.K. is indebted to the Baden-Württemberg Stiftung for the financial support of this research project by the Eliteprogramme for Postdocs. Financial support from the *Fonds der Chemischen Industrie* (FCI) is gratefully acknowledged. Prof. P. Roesky and Prof. A. K. Powell are thanked for the allocation of technical equipment, S. Lude for measuring the elemental analysis, and Dr. M. H. Klingele for helpful discussions. J.K. thanks Prof. I. Krossing and Prof. H. Hillebrecht for their generous and continuous support. Y.L. is grateful to Prof. A. K. Powell for her generous support. J.-F.L. and G.C. would like to thank the GIS-Advanced Materials in Aquitaine (AMA) and the Aquitaine Region for supporting the development of the ICPA (International Center of Photomagnetism in Aquitaine) platform at the ICMCB.

■ REFERENCES

(1) Hauser, A. *Top. Curr. Chem.* **2004**, *233*, 49−58.
(2) Klingele, J.; Kaase, D.; Klingele, M. H.; Lach, J. *Dalton Trans.* **2012**, *41*, 1397−1406.
(3) Guionneau, P.; Marchivie, M.; Bravic, G.; Létard, J.-F.; Chasseau, D. *Top. Curr. Chem.* **2004**, *234*, 97−128.
(4) Halcrow, M. A. *Chem. Soc. Rev.* **2011**, *40*, 4119−4142.
(5) Gütlich, P.; Hauser, A.; Spiering, H. *Angew. Chem.* **1994**, *106*, 2109−2141.
(6) Weber, B.; Bauer, W.; Pfaffeneder, T.; Dîrtu, M. M.; Naik, A. D.; Rotaru, A.; Garcia, Y. *Eur. J. Inorg. Chem.* **2011**, 3193−3206.
(7) Pfaffeneder, T. M.; Thallmair, S.; Bauer, W.; Weber, B. *New J. Chem.* **2011**, *35*, 691−700.
(8) Klingele, J.; Kaase, D.; Klingele, M. H.; Lach, J.; Demeshko, S. *Dalton Trans.* **2010**, *39*, 1689−1691.
(9) Decurtins, S.; Gütlich, P.; Köhler, C. P.; Spiering, H. *Chem. Phys. Lett.* **1984**, *105*, 1−4.
(10) Decurtins, S.; Gütlich, P.; Hasselbach, K. M.; Spiering, H.; Hauser, A. *Inorg. Chem.* **1985**, *24*, 2174−2178.
(11) Létard, J.-F.; Guionneau, P.; Rabardel, L.; Howard, J. A. K.; Goeta, A. E.; Chasseau, D.; Kahn, O. *Inorg. Chem.* **1998**, *37*, 4432−4441.
(12) Létard, J.-F.; Capes, L.; Chastanet, G.; Moliner, N.; Létard, S.; Real, J.-A.; Kahn, O. *Chem. Phys. Lett.* **1999**, *313*, 115−120.
(13) Marcén, S.; Lecren, L.; Capes, L.; Goodwin, H. A.; Létard, J.-F. *Chem. Phys. Lett.* **2002**, *358*, 87−95.
(14) Létard, J.-F.; Guionneau, P.; Nguyen, O.; Sánchez Costa, J.; Marcén, S.; Chastanet, G.; Marchivie, M.; Goux-Capes, L. *Chem.—Eur. J.* **2005**, *11*, 4582−4589.
(15) Létard, J.-F. *J. Mater. Chem.* **2006**, *16*, 2550−2559.
(16) Létard, J.-F.; Chastanet, G.; Guionneau, P.; Desplanches, C. In *Spin-crossover materials−properties and applications*; Halcrow, M. A., Ed.; John Wiley & Sons: Chichester, UK, 2012; in press.
(17) Shimamoto, N.; Ohkoshi, S.-S.; Sato, O.; Hashimoto, K. *Inorg. Chem.* **2002**, *41*, 678−684.
(18) Mohammed, R.; Chastanet, G.; Tuna, F.; Malkin, T. L.; Barrett, S. A.; Kilner, C. A.; Létard, J.-F.; Halcrow, M. A. *Eur. J. Inorg. Chem.* **2013**, *2013*, 819−831, DOI: 10.1002/ejic.201201100.
(19) Bonnet, S.; Molnár, G.; Costa, J. S.; Siegler, M. A.; Spek, A. L.; Bousseksou, A.; Fu, W.-T.; Gamez, P.; Reedijk, J. *Chem. Mater.* **2009**, *21*, 1123−1136.
(20) Cointe, M. B.-L.; Moussa, N. O.; Trzop, E.; Moréac, A.; Molnár, G.; Toupet, L.; Bousseksou, A.; Létard, J.-F.; Matouzenko, G. S. *Phys. Rev. B* **2010**, *82*, 214106/1−11.
(21) Matouzenko, G. S.; Létard, J.-F.; Lecocq, S.; Bousseksou, A.; Capes, L.; Salmon, L.; Perrin, M.; Kahn, O.; Collet, A. *Eur. J. Inorg. Chem.* **2001**, 2935−2945.
(22) Leita, B. A.; Neville, S. M.; Halder, G. J.; Moubaraki, B.; Kepert, C. J.; Létard, J.-F.; Murray, K. S. *Inorg. Chem.* **2007**, *46*, 8784−8795.
(23) Bréfuel, N.; Collet, E.; Watanabe, H.; Kojima, M.; Matsumoto, N.; Toupet, L.; Tanaka, K.; Tuchagues, J.-P. *Chem.—Eur. J.* **2010**, *16*, 14060−14068.
(24) Sato, T.; Nishi, K.; Iijima, S.; Kojima, M.; Matsumoto, N. *Inorg. Chem.* **2009**, *48*, 7211−7229.
(25) Bonnet, S.; Siegler, M. A.; Sánchez Costa, J.; Molnár, G.; Bousseksou, A.; Spek, A. L.; Gamez, P.; Reedijk, J. *Chem. Commun.* **2008**, 5619−5621.
(26) Chastanet, G.; Gaspar, A. B.; Real, J. A.; Létard, J.-F. *Chem. Commun.* **2001**, 819−820.
(27) Chastanet, G.; Carbonera, C.; Mingotaud, C.; Létard, J.-F. *J. Mater. Chem.* **2004**, *14*, 3516−3523.
(28) Rodríguez-Velamazán, J. A.; Carbonera, C.; Castro, M.; Palacios, E.; Kitazawa, T.; Létard, J.-F.; Burriel, R. *Chem.—Eur. J.* **2012**, *16*, 8785−8796.
(29) Sciortino, N. F.; Scherl-Gruenwald, K. R.; Chastanet, G.; Halder, G. J.; Chapman, K. W.; Létard, J.-F.; Kepert, C. J. *Angew. Chem.* **2012**, *124*, 10301−10305.
(30) Niel, V.; Thompson, A. L.; Goeta, A. E.; Enachescu, C.; Hauser, A.; Galet, A.; Munoz, M. C.; Real, J. A. *Chem.—Eur. J.* **2005**, *11*, 2047−2060.
(31) Krivokapic, I.; Enachescu, C.; Bronisz, R.; Hauser, A. *Inorg. Chim. Acta* **2008**, *361*, 3616−3622.
(32) Absmeier, A.; Bartel, M.; Carbonera, C.; Jameson, G. N. L.; Weinberger, P.; Caneschi, A.; Mereiter, K.; Létard, J.-F.; Linert, W. *Chem.—Eur. J.* **2006**, *12*, 2235−2243.
(33) Adams, C. J.; Muñoz, M. C.; Waddington, R. E.; Real, J. A. *Inorg. Chem.* **2011**, *50*, 10633−10642.
(34) Bauer, W.; Scherer, W.; Altmannshofer, S.; Weber, B. *Eur. J. Inorg. Chem.* **2011**, 2803−2818.
(35) Neville, S. M.; Leita, B. A.; Halder, G. J.; Kepert, C. J.; Moubaraki, B.; Létard, J.-F.; Murray, K. S. *Chem.—Eur. J.* **2008**, *14*, 10123−10133.
(36) Geldard, J. F.; Lions, F. *J. Org. Chem.* **1965**, *30*, 318−319.
(37) Hua, G.; Li, Y.; Fuller, A. L.; Slawin, A. M. Z.; Woollins, J. D. *Eur. J. Org. Chem.* **2009**, 1612−1618.
(38) Klingele, M. H.; Brooker, S. *Eur. J. Org. Chem.* **2004**, 3422−3434.
(39) Levine, R.; Sneed, J. K. *J. Am. Chem. Soc.* **1951**, *73*, 5614−5616.
(40) *The Cambridge Structural Database*, CSD version 5.33, Cambridge Crystallographic Data Centre, Cambridge, U.K.; November 2011.
(41) Shao, S.-C.; Liu, Z.-D.; Zhu, H.-L. *Acta Crystallogr. Sect. E* **2004**, *60*, m1815−m1816.

(42) Huang, X.-F.; Zhu, Y.-L.; Tang, L. *J. Coord. Chem.* **2011**, *64*, 1602−1607.
(43) Zhang, S.-P.; Shao, S.-C.; Liu, Z.-D.; Zhu, H.-L. *Acta Crystallogr. Sect. E* **2005**, *61*, m799−m800.
(44) Zhu, D.-R.; Song, Y.; Xu, Y.; Zhang, Y.; Shanmuga Sundara Raj, S.; Fun, H.-K.; You, X.-Z. *Polyhedron* **2000**, *19*, 2019−2025.
(45) Ma, C.-Y.; Guan, Y.-F.; Zhou, A.-J.; Wang, J.; Dong, W. *J. Coord. Chem.* **2010**, *63*, 3565−3575.
(46) Qi, L.; Zhu, D.-R.; Xie, D.-J.; Wu, Y.-F.; Shen, X. *Wuji Huaxue Xuebao−Chin. J. Inorg. Chem.* **2008**, *24*, 868−872.
(47) Hartmann, U.; Vahrenkamp, H. *Inorg. Chim. Acta* **1995**, *239*, 13−17.
(48) Moliner, N.; Muñoz, M. C.; Létard, S.; Létard, J.-F.; Solans, X.; Burriel, R.; Castro, M.; Kahn, O.; Real, J. A. *Inorg. Chim. Acta* **1999**, *291*, 279−288.
(49) Létard, J.-F.; Capes, L.; Chastanet, G.; Moliner, N.; Létard, S.; Real, J. A.; Kahn, O. *Chem. Phys. Lett.* **1999**, *313*, 115−120.
(50) Pillet, S.; Bendeif, E.-E.; Bonnet, S.; Shepherd, H. J.; Guionneau, P. *Phys. Rev. B* **2012**, *86*, 064106/1−11.
(51) Hauser, A. *Coord. Chem. Rev.* **1991**, *111*, 275−290.
(52) Hauser, A. *Comments Inorg. Chem.* **1995**, *17*, 17−40.
(53) Sheldrick, G. M. *Acta Crystallogr., Sect. A* **2008**, *64*, 112−122.
(54) Emmerling, F.; Orgzall, I.; Reck, G.; Schulz, B. W.; Stockhause, S.; Schulz, B. *J. Mol. Struct.* **2006**, *800*, 74−84.
(55) Bentiss, F.; Lagrenée, M. *J. Heterocycl. Chem.* **1999**, *36*, 1029−1032.

dx.doi.org/10.1021/ic400342m | *Inorg. Chem.* 2013, 52, 6000−6010